https://doi.org/10.5194/hess-2024-136
Preprint. Discussion started: 17 June 2024

Hydrology and Earth System Sciences
Discussions

Evaluating the effects of topography and land use change on hydrological signatures: a comparative study of two adjacent watersheds

Haifan Liu[1], Haochen Yan[1], Mingfu Guan[1*]
[1]Department of Civil Engineering, the University of Hong Kong, Hong Kong, China
Correspondence to: Dr. Mingfu Guan (mfguan@hku.hk)

Abstract. Watershed hydrological processes are significantly influenced by land use/land cover change (LULCC) and watershed characteristics such as topography. This study comparatively investigates the impacts of terrain slope and urbanization-driven LULCC on hydrological processes in two adjacent subtropical watersheds but with distinct terrain and land-cover conditions within the Greater Bay Area (GBA) of China. We developed an Integrated Surface-Subsurface Hydrological Model (ISSHM) using the Simulator for Hydrologic Unstructured Domains (SHUD), which was calibrated using data from river and groundwater flow monitoring stations in the watersheds. The calibrated model facilitated simulations to assess how terrain slope and LULCC affect surface runoff, subsurface flow, evapotranspiration (ET), and infiltration. Our results indicate that slope impacts hydrological processes differently in watersheds with varying characteristics. In mountainous areas, there are consistent high correlations between slope and annual surface runoff, infiltration, and subsurface flow across all watersheds. However, at lower elevations, the hydrological responses of steeper watersheds correlate weakly with local slope. Furthermore, urbanization (increase in impervious areas) has led to significant increases in annual surface runoff and significant decreases in annual infiltration and ET across all watersheds, especially in those with steeper slopes. On the other hand, in watersheds with gentler slopes, the annual increase in surface runoff is less than the percentage increase in impervious area, suggesting a buffering capacity of these flatter watersheds against urbanization. However, this buffering capacity is diminishing with increasing annual rainfall intensity.

1 Introduction

The effects of land use/land cover change (LULCC) and topographic variability on hydrological processes within a watershed are widely recognized as critical issues in hydrology (e.g., Bosch and Hewlett, 1982; O'Loughlin, 1986; Costa et al., 2003; Beven, 2011; Gwak and Kim, 2016; Larson et al., 2022; Sicaud et al., 2024). Urbanization has been demonstrated to significantly impact hydrological processes such as surface runoff, evapotranspiration (ET), infiltration, and subsurface flow by altering the conditions of the land surface (Olang and Fürst, 2011; Ayalew et al., 2015; Guan et al., 2015; Bai et al., 2020;

https://doi.org/10.5194/hess-2024-136
Preprint. Discussion started: 17 June 2024


Hydrology and Earth System Sciences
Discussions

Yan et al., 2023; Liang and Guan, 2024). Furthermore, it is evident that topographic characteristics have a direct influence on surface water flow paths and soil moisture, thereby affecting infiltration rates and groundwater recharge (Strahler, 1957; Hopp and McDonnell, 2009; Mirus and Loague, 2013; Smith et al., 2018; Yang et al., 2019; Zhang et al., 2022a). However, comprehending the diverse impacts of LULCC and topography on hydrological processes across disparate watersheds persists as a significant challenge, due to the variability in watershed characteristics and the nonlinear nature of hydrological responses (Niehoff et al., 2002; Brath et al., 2006; Thanapakpawin et al., 2007; Du et al., 2012; Pang et al., 2022; Yin et al., 2023; Guo et al., 2023; Yan et al., 2024). In order to address these challenges, researchers employ various methodologies to dissect and quantify these effects.

Statistical analysis techniques utilizing long-term monitoring data within a watershed are commonly used to examine the effects of LULCC (Beven et al., 2008; Liu et al., 2017; Zhang et al., 2021; Zhang et al., 2022b; Kumar et al., 2022). However, long-term changes in hydrological responses often reflect the combined impacts of climate change and LULCC, making it complicated to isolate the impacts of LULCC (Beven, 2011). The paired catchments approach is another statistical method commonly employed (Brown et al., 2005; Detty and McGuire, 2010; Yang et al., 2016; Van Loon et al., 2019), which compares monitoring data from two watersheds with different land cover but similar physical characteristics (Li et al., 2009; Shao et al., 2020). However, applying this approach in practice can be challenging due to the difficulty in identifying watersheds with similar physical characteristics. Furthermore, recent studies have indicated that LULCC-induced hydrologic alterations exhibit considerable spatial variability within watersheds, affecting upstream and downstream regions in disparate ways (Chu et al., 2010; Garg et al., 2017). In this regard, statistical analysis methods that rely on gauging datasets often lack detailed spatial resolution, employing methods that facilitate studies at finer spatial resolutions is essential for a comprehensive understanding of these variations.

Similar challenges exist when investigating the effects of topography on watershed-scale hydrological processes due to the diversity of geomorphic types and significant spatial variability within watersheds. One area where significant progress has been made is the prediction of hydrologic connectivity through topographic indices to study rainfall-runoff responses in watersheds (Jencso and McGlynn 2011). Topographic indices have become valuable tools for predicting soil moisture and identifying saturated zones. Two successful examples are topographic wetness index (TWI; Beven and Kirkby, 1979; Sørensen et al., 2006) and height above the nearest drainage (HAND; Nobre et al., 2011; Gao et al., 2019; Fan et al., 2019). However, some studies reported TWI and groundwater levels exist distinct relations at different locations (Detty and McGuire, 2010; Rinderer et al., 2014). Furthermore, the simulation results of HAND are highly depend on the pattern of observed saturated zones and it perform better at gentler watersheds (Nobre et al., 2011; Gao et al., 2019). In addition, the predictive accuracy of

https://doi.org/10.5194/hess-2024-136
Preprint. Discussion started: 17 June 2024


Hydrology and Earth System Sciences
Discussions

these indices decreases under dynamic conditions, such as at the onset of rainfall events (Seibert et al., 2003; Jarecke et al., 2021).

Recent studies have shown that hydrological models based on the Richards equation not only simulate surface-subsurface water interactions on hillslopes but also accurately describe hydrological processes under varying temporal conditions (Camporese et al., 2019). The Integrated Surface-Subsurface Hydrological Model (ISSHM) is a type of Richards equation-based fully distributed hydrological model (Shen and Phanikumar, 2010; Maxwell et al., 2014; Fatichi et al., 2016). Despite being relatively new compared to other hydrological models, the ISSHM has demonstrated significant capabilities in addressing the whole system of processes at watershed scales (Niu et al., 2017; Yu et al., 2022; Zanetti et al, 2024). By dividing the land surface into grids, such models can represent the spatial variability of hydrological processes with high spatial accuracy. They can also be solved with higher temporal accuracy by applying differential solutions to the physical governing equations. Unlike monitoring data analysis methods, ISSHMs allow hydrologists to assess the impact of specific factors by implementing designed scenarios and evaluating them across a comprehensive range of spatial and temporal scales. In recent years, ISSHMs have been proven valuable for assessing LULCC and topographic impacts at the watershed scale. For instance, Im et al. (2009) used the MIKE SHE model to show that urbanization increased total runoff by 5.5% and overland flow by 24.8% in a watershed. Zhang et al. (2022a) explored how topography influences subsurface flow with the HydroGeoSphere, revealing that topography plays a significant role in controlling penetration depths and stagnant zones.

While some studies have investigated the effects of LULCC and topography using the ISSHM approach, they are mainly based on single and spatially homogeneous watersheds, hindering comparative studies. Herein, we showcase the behavior of paired watersheds with heterogeneous patterns of both terrains and land cover, but are geographically adjacent to be compared under the same subtropical climate regime. We simulate the hydrological processes of the two watersheds in the Greater Bay Area (GBA), a crucial economic zone in China, using the Simulator for Hydrologic Unstructured Domains (SHUD) as an ISSHM. It examines the influences of terrain slope and urbanization-driven LULCC on the hydrological components of surface runoff, subsurface flow, ET, and infiltration at both daily and annual scales.

2 Study site

The study focuses on two neighboring watersheds within the Shenzhen River and Bay Basin (SRBB) in the Greater Bay Area (GBA)—the Ng Tung River Watershed (NTRW) in Hong Kong and the Buji River Watershed (BJRW) in Shenzhen (Figs. 1a and 1b). The NTRW encompasses an area of 70.7 km², while the BJRW covers 66.3 km². Situated in a subtropical region, the SRBB experiences an average annual temperature of 23.3°C and receives a substantial amount of precipitation, averaging 1933 mm annually, with significant inter-annual variability. Notably, about 86% of this precipitation falls during the monsoon season

https://doi.org/10.5194/hess-2024-136
Preprint. Discussion started: 17 June 2024

Hydrology and Earth System Sciences
Discussions
Open Access
EGU

(April–September), with the region experiencing an average of 130 rainy days per year. The intensity of daily rainfall during this period can be significant, reaching 289 mm and 382 mm for the 10-year and 50-year return period events, respectively.

Despite their proximity and similar climatic conditions, the NTRW and BJRW exhibit distinct differences in topography and land use patterns. The NTRW is characterized by steep slopes, with an average gradient of 12.3° and elevation variations ranging from 0.5 to 611.6 m (average elevation 97.1 m). In contrast, the BJRW features relatively flatter terrain, with an average slope of 7.5° and elevation ranging from 0.5 to 435.3 m (average elevation 70.6 m) (Fig. 1c). These watersheds reflect the rapid urbanization occurring in both Shenzhen and Hong Kong since the 1980s; however, urbanization has progressed more rapidly in the BJRW. Initially, the BJRW had limited construction areas with forests predominating (Cheng et al., 2023). By 2020, built-up land in the BJRW had increased to 71%, while in the NTRW, forests remain dominant and built-up areas constitute 37% of the land (Fig. 1d).

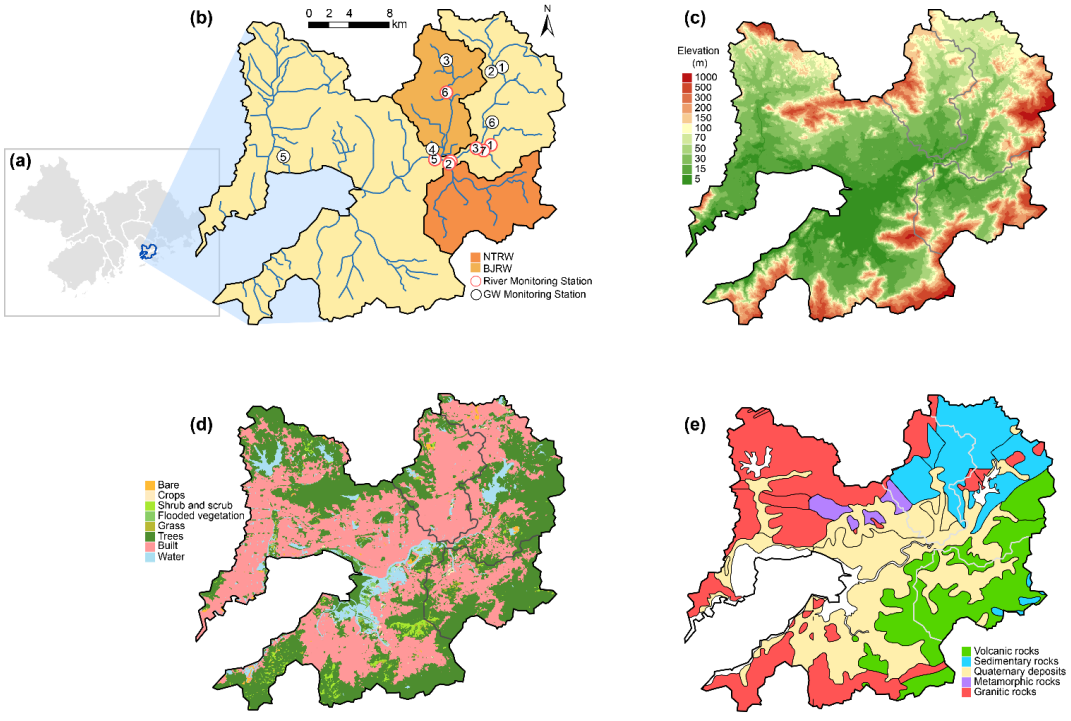

Figure 1. Location and characteristics of the Ng Tung River Watershed (NTRW) and Buji River Watershed (BJRW): (a) location of the Shenzhen River and Bay Basin (SRBB) within the Greater Bay Area (GBA), (b) location of the NTRW (dark orange) and BJRW (light orange) within the SRBB (yellow), along with channels (blue), calibration river monitoring stations (numbered 1–7, red circles), and calibration groundwater monitoring stations (numbered 1–6, black circles), (c) DEM (FABDEM V1-2), (d) land cover map of 2020, (e) geological map.

https://doi.org/10.5194/hess-2024-136
Preprint. Discussion started: 17 June 2024

3 Methodology

3.1 Hydrological model

The hydrological model employed in this study is SHUD (Shu et al., 2020), which evolved from the well-known Penn State Integrated Hydrologic Model (PIHM; Qu and Duffy, 2007; Kumar, 2009; Kumar et al., 2009). SHUD is an open-source model that incorporates a user-friendly data preprocessing toolkit, rSHUD (Shu et al., 2024), designed to simplify tasks such as grid partitioning, data integration, and model setup, addressing common challenges faced by hydrologists when working with ISSHMs. By integrating the parallel programming framework OpenMP, SHUD achieves high computational efficiency and has demonstrated superior robustness in solving problems at the watershed scale compared to PIHM, thus confirming its effectiveness in hydrological modeling (Shu et al., 2020).

As illustrated in Fig. 2, the hydrological processes simulated by SHUD include rainfall, surface water ponding storage, surface water infiltration, surface runoff, ET, changes in unsaturated layer moisture, groundwater flow, and river flow processes. The model represents the land domain using unstructured triangular elements and trapezoid segments for the river network. Each triangular element is vertically discretized into three layers: the top layer represents the land surface, the middle layer represents the unsaturated zone, and the bottom layer represents the saturated aquifer. The model employs the finite volume method to spatially discretize the partial differential equations of hydrological states into ordinary differential equations, enabling detailed simulation of hydrological dynamics.

For a more comprehensive understanding of the four hydrological processes analyzed in this study, we provide the relevant assumptions and computational formulas used in SHUD in Appendix A. Further details on the mathematical and algorithmic structure of SHUD are available in the referenced papers (Shu et al., 2020; Shu et al., 2024) and on the SHUD Book website (SHUD Book, 2024).

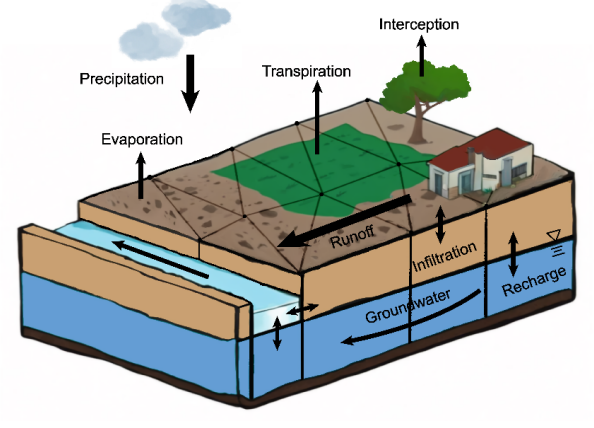

Figure 2. Model schematic of hydrological processes in the SHUD model.

https://doi.org/10.5194/hess-2024-136
Preprint. Discussion started: 17 June 2024

Hydrology and Earth System Sciences
Discussions
Open Access
EGU

3.2 Data collection and model setup

We set up the model domain as the entire SRBB, rather than focusing solely on its smaller two watersheds. This decision was driven by two strategic considerations. Firstly, the limited availability of monitoring data within the two watersheds necessitated a broader spatial framework to ensure a comprehensive dataset for robust hydrological analysis. Secondly, the similar characteristics of geology (Fig. 1e), soil (Fig. 3d), and vegetation (Fig. 3e) across the SRBB and its subbasins supported the feasibility of this extensive modeling approach. The SRBB, covering an area of 596 km², was discretized into 6,602 triangular meshes. Specifically, the NTRW and the BJRW were represented by 819 and 793 triangular grids, respectively (Fig. 3a). In the model, the outer boundary of the SRBB was designated as a zero-flow boundary, meaning no water flows across this boundary. Additionally, the land and river boundaries along the concave boundary in the southwestern part of the basin were set as a fixed head value, corresponding to the local sea level. This fixed-head boundary was established at 1.5 m, based on annual tidal observations from the Hong Kong Observatory (HKO). While this fixed-head approximation does not account for the precise daily tidal fluctuations, it represents a reasonable compromise for hydrological modeling purposes. Given that the two watersheds are situated significantly inland from the ocean, their hydrological processes are minimally affected by tidal variations.

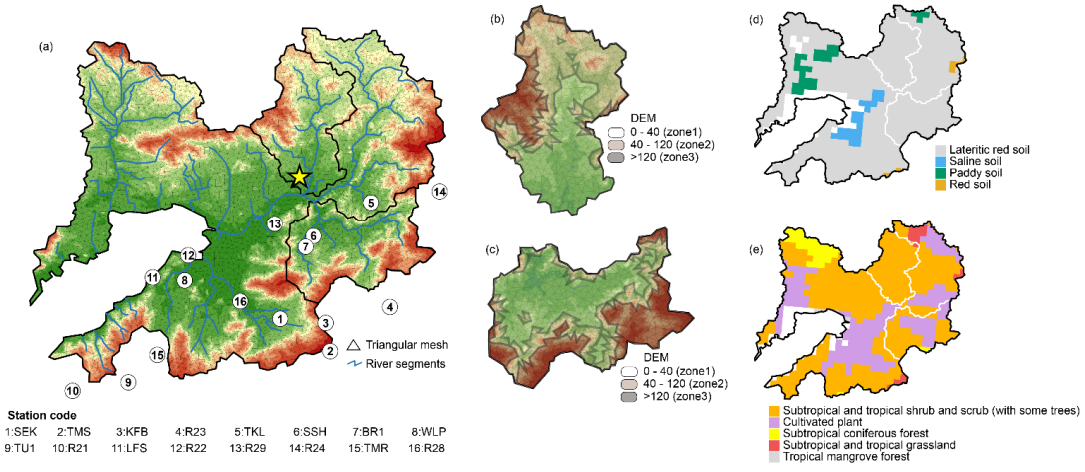

Figure 3. Map of meteorological site locations and triangular meshes of two watersheds, black circles (numbered 1-16) represent rainfall sites located in Hong Kong, and yellow star represent the Shenzhen Meteorological Station (SMS), (a) three zones delineated for BJRW (b) three zones delineated for NTRW (c), soil map (d), and vegetation map (e).

The Digital Elevation Model (DEM) for the study area was sourced from the FABDEM V1-2 dataset (Neal and Hawker, 2023) and offers a resolution of 30 meters. Land cover data for 2020, with a spatial resolution of 10 meters, were acquired from the Dynamic World Project via Google Earth Engine (Brown et al., 2022). Data on soil types and vegetation were obtained

https://doi.org/10.5194/hess-2024-136
Preprint. Discussion started: 17 June 2024

Hydrology and Earth System Sciences
Discussions

from the Data Center for Resources and Environmental Sciences at the Chinese Academy of Sciences (RESDC, 2024), and geological information was sourced from the China Geological Survey (GeoCloud, 2024). Satellite imagery was utilized to determine river channel widths. Determining the appropriate soil depth remains a significant challenge, and as highlighted by Fan et al. (2019), weathering fractures notably influence hydrological activities. Based on the geological data from the study site, extensive weathering is noted in the mountainous regions. Consequently, the aquifer depth was modeled to vary gradually from 18 meters in the upslope areas to 9 meters downstream.

Additionally, driving force data were collected for two distinct periods. The first period, from 2020 to 2021, included hourly meteorological data from the Shenzhen Meteorological Station (SMS), provided by the Meteorological Bureau of the Shenzhen Municipality. This dataset included records of precipitation, temperature, relative humidity, and wind speed. Hourly precipitation data for the same period were also gathered from 16 additional gauging sites in Hong Kong, sourced from the HKO (Fig. 2a). The second period, from 1993 to 2021, involved collecting precipitation data from the R29 station via the HKO. Moreover, monitoring data of daily river discharge from seven stations and daily or weekly groundwater table depths from six stations were gathered from the Water Authority of the Shenzhen Municipality for the period of 2020–2021. A comprehensive summary of all datasets and related information is provided in Table 1.

Table 1. Summary of collected datasets and related information.

Data	Source	Resolution	Time period	Purpose
DEM	FABDEM V1-2	30 m		
Land cover type	Dynamic World Project	10 m	2020	
Soil type	RESDC	1000 m		Model mesh grid attributes set up
Geology	China Geological Survey (GeoCloud)	100 m		
River characteristics	Google Earth			
Meteorological data of the Shenzhen Meteorological Station (SMS)	Meteorological Bureau of the Shenzhen Municipality	Hourly	2020–2021	(1) Model calibration phase driving force inputs; (2) Model scenarios 1 and 2 driving force inputs
Precipitation of 16 Hong Kong stations	Hong Kong Observatory (HKO)	Hourly	2020–2021	Model calibration phase driving force inputs
Precipitation of the R29 station	Hong Kong Observatory (HKO)	Hourly	1993–2021	Model scenarios 3 and 4 driving force inputs
Streamflow monitoring data of 7 sites	Water Authority of the Shenzhen Municipality	Daily	2020–2021	Model calibration
Groundwater table depth monitoring data of 6 sites	Water Authority of the Shenzhen Municipality	Daily or weekly	2020–2021	

https://doi.org/10.5194/hess-2024-136
Preprint. Discussion started: 17 June 2024


Hydrology and Earth System Sciences
Discussions

3.3 Model calibration

We employed rainfall data from 17 sites covering the period from 2020 to 2021 to drive the model during the calibration process. To distribute the rainfall data effectively across all 17 sites, we utilized the Thiessen multi-polygon method, allocating the data to corresponding triangular grids. Due to limitations in data availability, meteorological parameters such as temperature, relative humidity, and wind speed were sourced solely from the SMS for the entire basin. The initial setup of the model parameters was informed by field data, the general features of the model structure, and past modeling experience. The model underwent multiple spin-up sessions using 2020 meteorological data to establish an initial condition that closely mirrors the monitoring datasets. Given the heterogeneity of the basin, effective auto-calibration was challenging, leading to a preference for manual calibration as a common practice for ISSHMs (Shi et al., 2014; Thornton et al., 2022; Brandhorst and Neuweiler, 2023). We leveraged previous uncertainty analysis and parameter sensitivity studies (Baroni et al., 2010; Song et al., 2015; Liu et al., 2020) to select the most crucial parameters for this hands-on calibration process. Monitoring data from the entire period were utilized for calibration, focusing on enhancing model performance. Our calibration efforts concentrated on both streamflow and groundwater table depths to ensure a comprehensive evaluation of the model. The selected parameters and the final calibrated results are discussed in Sect. 4.1.

3.4 Scenario design and evaluation methods

We developed four modeling scenarios differentiated by time span and land use pattern (Table 2). Scenarios 1 and 2 analyze hydrological processes at daily and annual temporal resolutions, respectively, using continuous meteorological data provided by the SMS for the years 2020–2021. These scenarios aim to determine how watershed topography and urbanization conditions influence daily and annual hydrological responses. Scenarios 3 and 4 extend the analysis to a 29-year period (1993–2021), utilizing rainfall data from the R29 station. This approach enriches our understanding of how annual rainfall variability influences topographic slope and LULCC on hydrological processes.

For the LULCC assessment, we considered two land use patterns: Historical Land Use (HLU) and Current Land Use (CLU). The HLU pattern involves reverting all built-type land uses in both watersheds to their pre-construction conditions, corresponding to the forest type evident in the 1979 satellite images from Google Earth. The CLU pattern reflects the land use as of 2020.

To isolate the impact of slope from LULCC effects, we analyzed slope impacts within the two watersheds exclusively under the HLU pattern. We conducted a thorough examination of model outputs across three distinct elevation zones within the watersheds. Zone 1 encompasses low-elevation regions with DEM values below 40 m, primarily consisting of flat areas.

https://doi.org/10.5194/hess-2024-136
Preprint. Discussion started: 17 June 2024

Hydrology and Earth System Sciences
Discussions

Zone 2 includes areas with DEM values ranging from 40 m to 120 m, situated at the foothills of the mountains. Zone 3 comprises primarily high-elevation regions with DEM values exceeding 120 m (Figs. 3b and 3c).

Table 2. Designed four scenarios.

Scenario	Driving force inputs time span	Land use pattern
1	2020–2021	HLU
2	2020–2021	CLU
3	1993–2021	HLU
4	1993–2021	CLU

In this study, the model outputs are exclusively positive, indicating water outflow, and are measured in meters to represent the depth of outflow over a specified period within each local grid. We used the Spearman rank correlation method (Seibert et al., 2003; Hauke and Kossowski, 2011) to analyze the results of Scenario 1, quantifying the relationship between the slope and four model outputs. To assess the impact of LULCC, we applied the Kolmogorov-Smirnov (KS) two-sample test (Lilliefors, 1967) between Scenario 1 and Scenario 2. In all simulations, the output results are recorded at a one-day time interval. When analyzed on a daily scale, the results can be directly examined. For annual evaluations, the output results are aggregated by year. Detailed equations used for these assessments are provided in Appendix B to facilitate comprehensive understanding. To explore potential variations in the impact of slope due to annual rainfall fluctuations, we established a simple linear regression model. This model was used to examine the correlation between 29-year annual rainfall data and the Spearman correlation coefficients derived from Scenario 3. Additionally, a separate simple linear regression model was implemented to assess the relationship between 29-year annual rainfall and KS test values between Scenario 3 and Scenario 4. This approach aims to evaluate how annual rainfall fluctuations might influence LULCC.

4 Results and discussion

4.1. Model performance

Due to spatial heterogeneity within the watersheds, the calibrated values for each parameter are formed as a matrix. For clarity, only the median values is displayed (Table 3). The first four parameters, K_s, θ_{ss}, α and β, are primarily associated with the vadose zone and significantly influence the hydraulic processes in the soil layer. The last three parameters K_g, θ_{gs} and θ_{gr}, govern the hydraulic processes in the aquifer layer. All these parameters fall within reasonable ranges, as supported by previous studies (Das, 1990; Freeze and Cherry, 1979; Bear, 2013; Van Genuchten, 1980).

Figures 4a–c display the hydrographs of daily simulated and observed streamflow at various river gaging stations within the BJRW (Site 6; Fig. 4c), at the upstream of the watersheds (Site 1; Fig. 4a), and at the downstream of the watersheds (Site

https://doi.org/10.5194/hess-2024-136
Preprint. Discussion started: 17 June 2024

Hydrology and Earth System Sciences
Discussions

2; Fig. 4b), respectively. The Nash-Sutcliffe Efficiency (NSE) indices, computed for the entire simulation period, demonstrate satisfactory model performance, except for Site 2 where the observed dataset shows daily fluctuations in river flow during rain-free periods due to tidal influences. Therefore, for such sites, we specifically calibrated the discharge during rainy days and calculated the NSE index using data from those days. The simulation results exhibit satisfactory performance with NSE indices greater than 0.5, indicating a reasonable accuracy in streamflow predictions.

Furthermore, the monthly calibration results reinforce the robust performance of the calibrated model, exhibiting R^2 values exceeding 0.6 (Figs. 4d–f; Moriasi et al., 2007). This strong correlation suggests a consistent and reliable model behavior over a longer time scale. Figures 4g–i present the comparisons between the simulated and observed groundwater data. It is challenging to evaluate the assessment indices of groundwater calibration for such long durations. However, our calibration outcomes indicate a marked concordance between the model outputs and observed data trends, and the modeled groundwater table depth closely aligns with the measured depths, underscoring the model's accuracy in reflecting actual groundwater conditions. Overall, the model exhibits satisfactory performance on both surface and subsurface water flows. Additional sites' calibration results are available in Fig. C1.

Table 3. Refined parameters for the watershed after calibration.

Parameter	Description	Allowable value range	Median value after calibration	Unit
K_s	Soil saturated infiltration conductivity	10^{-3}–10^{4}	0.045	m day^{-1}
θ_{ss}	Soil saturated water content	0.25–0.7	0.531	-
α	van Genuchten parameter	>0	5.23	m^{-1}
β	van Genuchten parameter	>1	1.29	-
K_g	Groundwater hydraulic conductivity	10^{-5}–10^{4}	2.6	m day^{-1}
θ_{gs}	Groundwater saturated water content	0.0–0.5	0.3	-
θ_{gr}	Groundwater residual water content	0.0–0.5	0.01	-

https://doi.org/10.5194/hess-2024-136
Preprint. Discussion started: 17 June 2024

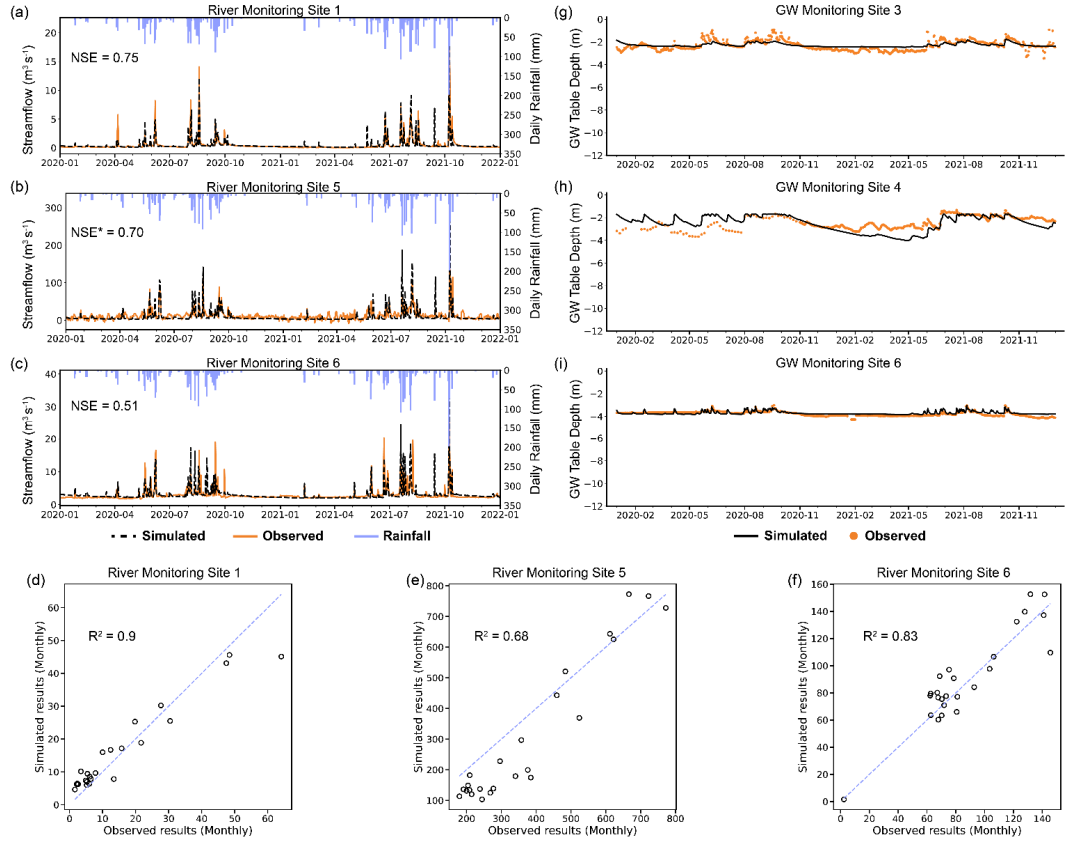

Figure 4. Calibration performance of SHUD model across daily river discharge in the river monitoring sites 1, 5 and 6 (a)–(c), and monthly river discharge in the river monitoring sites 1, 5 and 6 (d)–(f), and groundwater table depth in the groundwater monitoring sites 3, 4 and 6 (g)–(i).

4.2 Daily and annual scale hydrological responses

4.2.1 Stronger correlation between slope and daily subsurface flow

Figure 5 depicts the correlation between four hydrological processes and terrain slope on a daily scale, with all depicted markers being statistically significant (p-value ≤ 0.05). The analysis primarily emphasizes slope, but also explores the influence of daily rainfall to provide additional insights. The Spearman correlation analysis indicates slight correlation coefficients between surface runoff, infiltration, and slope, which lie between -0.2 and 0.2 in all zones of the two watersheds. In contrast, coefficients associated with daily rainfall range from -0.6 to 1. Notably, during rainy days, daily subsurface flow demonstrates a more pronounced correlation with slope (coefficients between -0.4 and 0.2) than with daily rainfall (coefficients between -0.2 and 0.2). Specifically, in Zone 1, a positive correlation is observed between daily subsurface flow and slope, while Zones 2 and 3 exhibit a negative correlation.

https://doi.org/10.5194/hess-2024-136
Preprint. Discussion started: 17 June 2024

Hydrology and Earth System Sciences
Discussions

Consistent with the findings in existing literature, this result underscores the critical role of topographical factors in influencing groundwater dynamics during rainfall events (Hopp and McDonnell, 2009; Detty and McGuire, 2010; Jencso and McGlynn, 2011; Singh et al., 2021). The observed negative correlations between slope and subsurface flow in the middle and high elevations of the two watersheds can be attributed to the predominantly accretive state of groundwater in these areas. In these higher elevations, lower slopes contribute to enhanced groundwater retention and accumulation, thus enhancing subsurface flow. Conversely, in the lower elevations of both watersheds, the positive correlation between slope and subsurface flow may be explained by the tendency of groundwater to move towards surface water more readily after rainfall events. The flatter topography in these lower areas facilitates this transferring process, thereby reducing the total amount of subsurface flow retained within the soil.

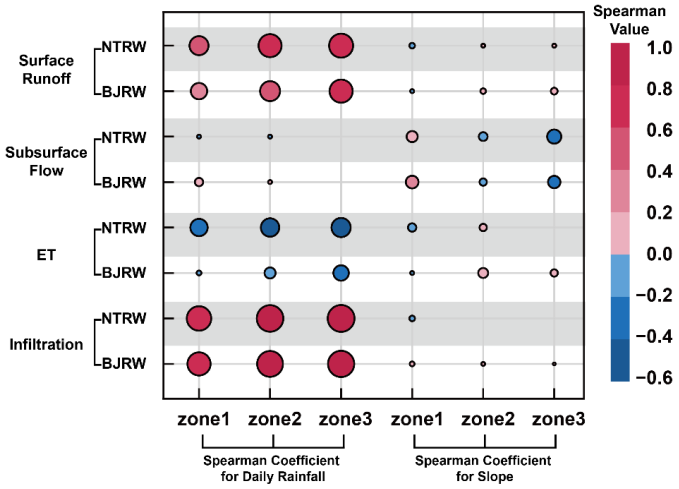

Figure 5. Comparative analysis of slope influence and daily rainfall on four hydrological variables. Marker size denotes the absolute value of the Spearman correlation coefficients, while marker color indicates the direction of the relationship between slope or rainfall and the four model outputs. Generally, red represents a positive correlation, whereas blue denotes a negative correlation.

4.2.2 Faint slope-flow relationship in NTRW's lower zone

Figure 6 presents the comparative results of terrain slope at daily and annual scales. The findings suggest that slope has a more pronounced relationship with annual surface runoff, subsurface flow, and infiltration at higher elevations compared to daily scales, highlighting the pivotal role of slope in redistributing water post-rainfall events. This aligns with the observations by Seibert et al. (2003) and Rinderer et al. (2014), who noted that topographic indices more accurately reflect hydrological responses under steady-state conditions. Specifically, Rinderer et al. (2014) reported from their analysis of data from 51 groundwater wells in a Swiss catchment that the ability of the TWI to predict water table distributions diminishes under unsteady conditions.

https://doi.org/10.5194/hess-2024-136
Preprint. Discussion started: 17 June 2024

Hydrology and Earth System Sciences
Discussions
Open Access
EGU

263 Concerning the direction of correlation, surface runoff in mountainous areas exhibits a positive correlation with slope at
264 both daily and annual scales, whereas subsurface flow shows a negative correlation. On a daily scale, this pattern may be
265 primarily due to the direct influence of slope on water flow paths. However, on an annual scale, variations in infiltration play
266 a more substantial role (Table C1). The results indicate that in both watersheds, infiltration rates decrease at higher elevations
267 as slopes increase, leading to increased surface water runoff and reduced subsurface flow in areas with steeper slopes.

268 When examining annual flow processes at lower elevations, a significant correlation between terrain slope and
269 hydrological behavior is evident in the gently sloping BJRW. In contrast, such correlation is notably faint in the steeper NTRW.
270 This disparity may be attributed to the fact that water flow in steeper watersheds tends to be quicker (Fan et al., 2019; Singh
271 et al., 2021), leading to hydrological processes at lower elevations being primarily influenced by rapid upstream inflows rather
272 than the local topography. On the other hand, the gentler slopes of other watersheds facilitate slower flow processes, allowing
273 topographic features at lower elevations to continuously influence water flow paths over time, thus maintaining a consistent
274 hydrological impact.

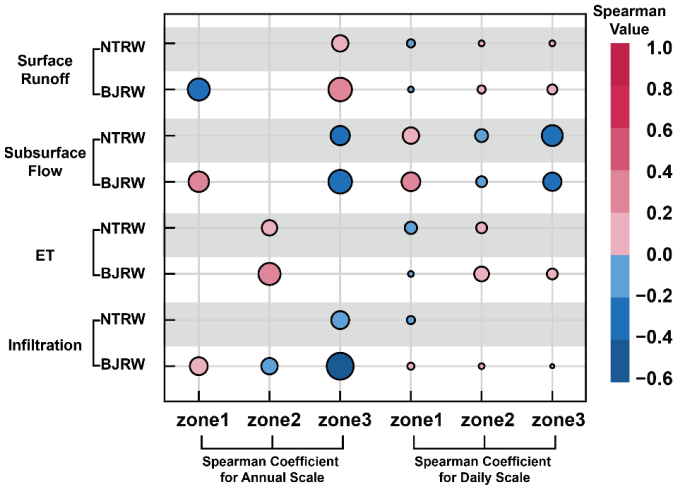

275

276 **Figure 6.** Comparison of hydrological responses to slope variability on annual and daily scales in NTRW and BJRW.

277 **4.2.3 Dominant impact of LULCC on daily infiltration**

278 Figure 7 illustrates the absolute mean differences in hydrologic outputs between the HLU and CLU patterns for each grid cell.
279 Employing the KS statistic, significant alterations in the cumulative distribution function (CDF) of daily hydrologic outputs
280 were identified, highlighting the substantial impacts of LULCC. Among the hydrological processes examined, daily infiltration
281 exhibits the most pronounced and widespread differences, underscoring the dominant influence of LULCC.

https://doi.org/10.5194/hess-2024-136
Preprint. Discussion started: 17 June 2024

Hydrology and Earth System Sciences
Discussions

When considering only absolute mean differences, surface runoff and subsurface flow are identified as the second and third most influenced processes, respectively. However, when focusing exclusively on the results from the KS statistical test, ET emerges as the second most affected process. This indicates that land use changes significantly alter ET patterns on rainy days, despite the smaller mean differences observed.

This finding aligns with the results of Chu et al. (2010) and Diem et al. (2021), which underscore the extensive impact of urbanization on surface runoff through changes in infiltration. Notably, the distribution of affected subsurface flow in both watersheds closely correlates with the areas exhibiting the most significant changes in infiltration. Compared to the steeper NTRW, the flatter BJRW shows broader changes in subsurface flow as a result of LULCC. This disparity likely stems from the prolonged water-soil contact in flatter terrains, which enhances infiltration. Consequently, this enhanced infiltration process leads to a more extensive distribution of soil moisture throughout the watershed, influencing both surface and subsurface hydrological dynamics.

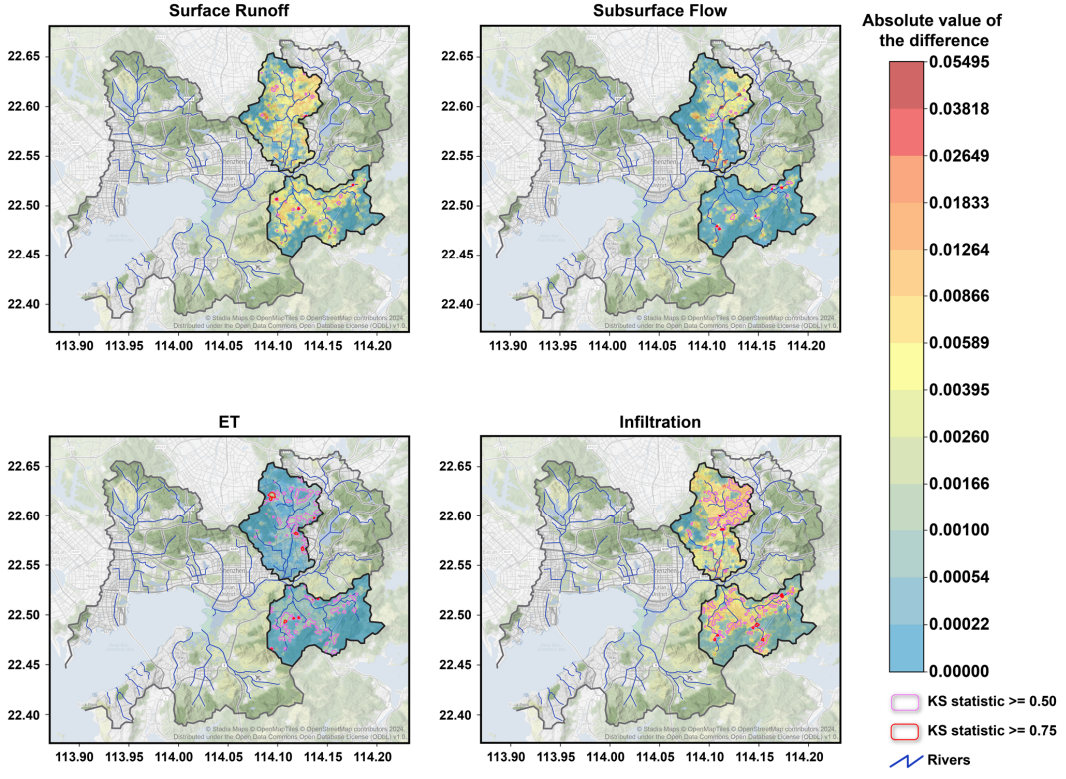

Figure 7. Map of absolute mean differences at each grid between HLU and CLU patterns, with significant variations in daily hydrologic output CDFs marked according to the KS statistic. The color coding represents the absolute value of the differences in these outputs, and the pink and red circles indicate areas where the KS statistic is significant.

https://doi.org/10.5194/hess-2024-136
Preprint. Discussion started: 17 June 2024


Hydrology and Earth System Sciences
Discussions

4.2.4 NTRW shows more sensitivity to LULCC

The KS test indicates statistically significant changes in all four hydrological outputs after urbanization, with all p-values below 0.05 (refer to Fig. 8). The results depict an increase in annual surface runoff and reductions in subsurface flow, ET, and infiltration following urbanization. This aligns with findings from Shao et al. (2020), who used a process-based hydrological model to examine the response of surface runoff to LULCC in two adjacent watersheds in Texas, USA. They reported that urbanization leads to increased runoff, a finding consistent with our results.

Furthermore, the KS test results reveal relative consistency within each watershed for surface runoff, ET, and infiltration values. Specifically, in the NTRW, the KS values for surface runoff, ET, and infiltration are recorded at 0.39, 0.395, and 0.377, respectively. The corresponding values in the BJRW are 0.531, 0.583, and 0.615. However, subsurface flow shows lower KS values of 0.127 in the NTRW and 0.263 in the BJRW, suggesting that urbanization has a less impact on the annual subsurface flow process.

This minimal impact on subsurface water flow suggests that the slower dynamics of subsurface water may buffer the direct effects of urbanization at the annual scale. In the BJRW, where impervious surfaces account for 71% of the land cover change, the response of surface runoff, ET and infiltration is more pronounced (with KS values ranging from 0.531 to 0.615) compared to the NTRW, where impervious surfaces make up 37% of the change (with KS values ranging from 0.377 to 0.395).

It is noteworthy that in the BJRW, the KS values for surface runoff, ET, and infiltration are slightly lower than the percentage increase in impervious surfaces. This suggests that the flatter watershed may possess a natural ability to mitigate the effects of LULCC. This observation is supported by Zhou et al. (2015), who noted that flatter terrains tend to absorb changes more effectively due to prolonged water-soil contact times, which enhance infiltration and storage capacities. This capacity may help mitigate the more severe hydrological alterations typically associated with extensive urbanization.

https://doi.org/10.5194/hess-2024-136
Preprint. Discussion started: 17 June 2024

Hydrology and Earth System Sciences
Discussions

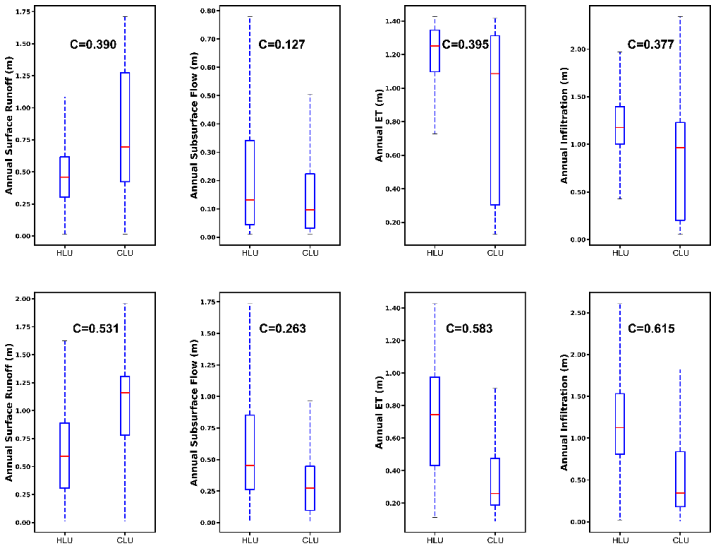

317

318 **Figure 8.** Box plots delineating the impacts of LULCC on the four annual outputs across all meshes within each watershed. The comparison
319 contrasts the outcomes under the HLU and CLU patterns. The top row displays the results of NTRW, while the second row displays the
320 results of BJRW. KS test values (C) are annotated, all p-values are less than 0.05.

321 **4.3 Variations with different annual rainfall amounts**

322 **4.3.1 Rainfall intensifies subsurface flow-slope relationship in BJRW's lower zone**

323 Figure 9 presents scatterplots and regression equations that analyze the correlation between annual precipitation and Spearman
324 statistic values from 1993 to 2021, highlighting outcomes that are statistically significant (p-value ≤ 0.05), as identified in Sect.
325 4.2.2. The analysis shows minimal changes in Spearman statistic values across most study areas; however, a notable variation
326 was observed in subsurface flow within Zone 1 of the BJRW, where a coefficient of 0.07 indicates that each 100 mm increase
327 in annual precipitation enhances the correlation between slope and subsurface flow by 0.007. This change corresponds to a
328 shift in the Spearman coefficient from 0.174 to 0.258 as annual rainfall increases from 1200 mm to 2400 mm. This observation
329 is supported by findings from Zhang et al. (2022a), who reported that under scenarios of higher precipitation and greater
330 hydraulic conductivity, the extent and permeation depth of the saturated zones beneath mountains exhibit a stronger correlation
331 with the terrain. This effect is likely due to increased precipitation levels raising the water table at lower elevations, thus
332 enhancing the relationship between slope and subsurface flow.

https://doi.org/10.5194/hess-2024-136
Preprint. Discussion started: 17 June 2024

Hydrology and Earth System Sciences
Discussions

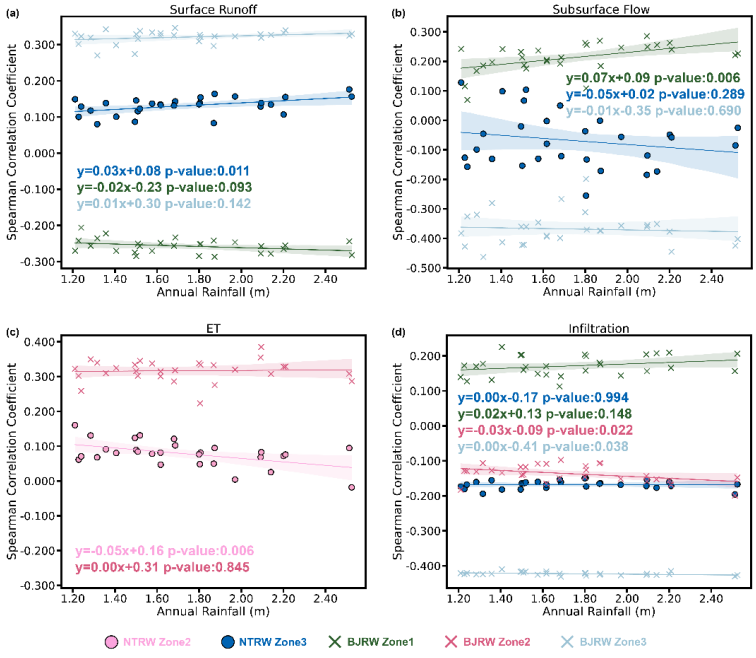

Figure 9. Scatter plots of Spearman statistic values of slope and four model outputs under 29 years of different annual rainfall amounts, with simple regression equations and shade area showing the 95% confident interval.

4.3.2 Rainfall intensifies the changes in groundwater caused by LULCC

Figure 10 presents scatter plots correlating KS test values for four hydrological outputs with 29 years of annual rainfall data, evaluating how the impacts of LULCC vary under different precipitation intensities. Our analysis highlights significant variability in the effects of LULCC across various annual rainfall amounts in the BJRW. Here, surface runoff and infiltration exhibit reduced variations before and after urbanization as annual rainfall increases, whereas variations in subsurface flow intensify. In the NTRW, significant changes are primarily observed in annual subsurface flow, which also shows increased variation with higher levels of annual precipitation. In scenarios where all surfaces are pervious, an increase in annual rainfall leads to gradually saturated soil moisture, thereby enhancing surface runoff and reducing water infiltration. This behavior mirrors observations on impervious surfaces. However, in environments predominantly composed of impervious surfaces, surface water cannot effectively infiltrate to form groundwater. This leads to a poor connectivity in saturated zones, thereby impeding the formation of subsurface flow. As annual rainfall increases, the differences in subsurface flow between land use patterns become more pronounced.

https://doi.org/10.5194/hess-2024-136
Preprint. Discussion started: 17 June 2024

Hydrology and Earth System Sciences
Discussions

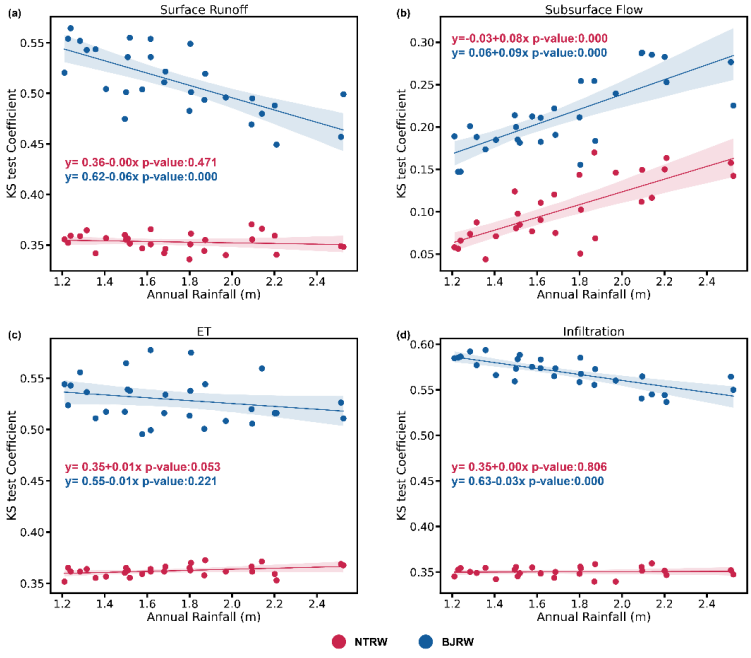

Figure 10. Scatter plots of KS test coefficients of LULCC and four model outputs under 29 years of different annual rainfall scenarios, with simple regression equations and shade area showing the 95% confident interval.

4.4 Limitations and future work

Our study provides valuable insights into the effects of topography and LULCC on hydrological processes across various spatiotemporal scales in different watersheds. Although the hydrological model used was comprehensively calibrated using observational data and demonstrated accurate predictive capabilities, several limitations warrant consideration. Firstly, the calibration of the model parameters was conducted manually using local data, which may not encompass the optimal parameter sets unidentified in this study. Furthermore, the inherent uncertainties associated with the monitoring data and the model structure were not thoroughly evaluated. Due to the complexity of ISSHMs and the significant amount of time required to thoroughly assess all uncertainties, such evaluations remain challenging but are necessary for advancing the field. Secondly, our study area is located in a subtropical humid region characterized by frequent rainfall and consistently moist soils. This geographical specificity may limit the generalizability of our findings to regions with different climatic conditions. Thirdly, the rainfall data utilized in this study only encompassed the typical range of precipitation for the region; extreme rainfall events, which may induce unique hydrological responses, were not investigated. The impact of such extreme conditions remains to be explored in future studies.

https://doi.org/10.5194/hess-2024-136
Preprint. Discussion started: 17 June 2024

Hydrology and Earth System Sciences
Discussions

5 Conclusions

Utilizing the ISSHM model, SHUD, this study explored the effects of topographical slope and urbanization-induced LULCC on surface runoff, subsurface flow, ET, and infiltration across various spatiotemporal conditions in two neighboring subtropical watersheds. In conclusion, this study confirms the complex and variable effects of topography and LULCC on hydrological processes across various watersheds, spatial locations within watersheds, and temporal scales. On a daily scale, slope is found to correlate with subsurface flow. However, on an annual scale, slope correlates with all hydrological processes, with the strongest correlation observed in mountainous regions. In flatter watersheds, prolonged soil-water interactions enhance infiltration and influence water redistribution, thus increasing the correlation between slope and surface runoff and subsurface flow, especially as annual precipitation increases. Our findings suggest that urbanization significantly increases surface runoff while decreasing infiltration and ET, with minimal impact on subsurface flow. Furthermore, watersheds with steeper slopes show a more pronounced response to urbanization, whereas those with gentler slopes mitigate the effects of LULCC on increased surface runoff. This phenomenon can be described as a buffering effect of gently sloping watersheds. However, this buffering effect diminishes as annual rainfall increases. This study underscores the need for hydrologic management strategies tailored to the specific topography and LULCC characteristics of each watershed. A comprehensive understanding of these factors is crucial for developing effective water resource management approaches that support sustainable development in these areas.

Appendix A: SHUD hydrological processes formulas

The comprehensive exposition of the governing equations for the SHUD is provided in Shu et al. (2020). Here, the emphasis is placed on expounding the equations that are relevant to the processes addressed in this study.

- *Infiltration.* SHUD adopts the Richards equation like most ISSHMs adopted to describe the infiltration process. While there are no general analytical solutions to the Richards equation, SHUD adopted the Green-Ampt infiltration equation (Eq. (A1)), which allows a simple form of Darcy's law to be used to calculate the infiltration rate q_i [LT^{-1}],

$$q_{\mathrm{i}} = K_{\mathrm{i}}\left(1 + \frac{h_{\mathrm{s}}}{D_{\mathrm{inf}}}\right) \quad \text{(A1)}$$

where h_{s} [LT^{-1}] is the ponding water height plus precipitation, D_{inf} [L] is the infiltration depth representing the top soil layer, K_i [LT^{-1}] is the effective infiltration conductivity, and it is a function of soil saturation ratio, soil properties, and h_{s}. The Green-Ampt method assumes that the infiltrating wetting front forms a sharp jump from a constant initial moisture content ahead of the front to saturation at the front.

https://doi.org/10.5194/hess-2024-136
Preprint. Discussion started: 17 June 2024


Hydrology and Earth System Sciences
Discussions

-*Evapotranspiration.* Potential evapotranspiration (PET) is computed using the Penman-Monteith equation (Eq. (A2)), while actual evapotranspiration (AET) is derived by multiplying PET with a soil moisture stress coefficient, determined by soil moisture content and groundwater table depth.

$$\lambda E = \frac{\Delta_e H + \rho_a c_p (e_s(T_z) - e_z)/r_a}{\Delta_e + \gamma(1 + r_c/r_a)}, \quad \text{(A2)}$$

where λ(=2.4710^6, Jkg^{-1}) is the latent heat of evaporation, E [LT^{-1}] is the PET rate, Δ_e is the slope of the saturation vapor pressure versus temperature curve, H is total available energy, ρ_a is the density of the air, c_p is the specific heat capacity of the air, $e_s(T_z)$ is the saturated vapor pressure at the height of z, e_z is the vapor pressure at the height of z, r_a and r_c are the two resistance coefficients, γ is the psychrometric constant.

- *Surface runoff.* The kinematic wave equation (Eq. (A3)) is used to approximate the surface runoff in the SHUD,

$$\frac{\partial h}{\partial t} = -\frac{\partial (vh)}{\partial x} - \frac{\partial (vh)}{\partial y} + r, \quad \text{(A3)}$$

where h [L] represents the average depth of flow, v [LT^{-1}] is the flow velocity, and r [LT^{-1}] is a rate of addition or loss of water caused by precipitation, infiltration and evaporation. The relationship between v and h is represented by the Manning equation (Eq. (A4)),

$$v = -\frac{S_0^{\frac{1}{2}} h^{\frac{3}{5}}}{n}, \quad \text{(A4)}$$

where S_0 [-] is the surface slope, n [TL$^{-1/3}$] is the Manning roughness.

- *Subsurface flows.* The SHUD applies the Richards equation (Eq. (A5)) to describe both saturated and unsaturated flows, and the water density is assumed to be constant,

$$\frac{\partial \theta}{\partial t} = \frac{\partial}{\partial x}\left[K_x(\theta)\frac{\partial \Phi}{\partial x}\right] + \frac{\partial}{\partial y}\left[K_y(\theta)\frac{\partial \Phi}{\partial y}\right] + \frac{\partial}{\partial z}\left[K_z(\theta)\frac{\partial \Phi}{\partial z}\right], \quad \text{(A5)}$$

where θ [-] is volumetric moisture content, $K_x(\theta)$ [LT^{-1}], $K_y(\theta)$ [LT^{-1}], and $K_z(\theta)$ [LT^{-1}] indicate hydraulic conductivity depends on direction and is treated as a function of θ, Φ [L] is the total potential ($\Phi = \psi + z$ where ψ [L] is the capillary potential and z is the elevation above the datum). The SHUD utilizes the van Genuchten functions to solve the relationship for soil moisture content, capillary potential, and hydraulic conductivity.

Appendix B: Assessment equations

The Spearman rank correlation method evaluates the strength and monotonic nature of relationships between two variables without relying on assumptions regarding data distribution or residuals. The KS two-sample test compares two samples to

https://doi.org/10.5194/hess-2024-136
Preprint. Discussion started: 17 June 2024

Hydrology and Earth System Sciences
Discussions

determine if they are drawn from the same distribution, without assumptions about the underlying distribution. The KS statistic is the maximum absolute difference between the CDFs of the two data vectors.

For the daily scale analysis, we focused on positive model outputs during rainy days (precipitation ≥ 0.1 mm per day). We employed matrix **D** for each zone (Zone 1 to Zone 3) to assess daily outputs related to slope angle for each grid (Eqs. (B1) and (B2)).

$$\mathbf{D} = \begin{bmatrix} \mathbf{W}_1 \\ \vdots \\ \mathbf{W}_N \end{bmatrix}, \tag{B1}$$

$$\mathbf{W}_n = \begin{bmatrix} y_{1n} & p_1 & s_n \\ \vdots & \vdots & \vdots \\ y_{in} & p_i & s_n \end{bmatrix} \tag{B2}$$

In matrix **D**, each row $\mathbf{W}_n$ (n=1, 2, …, N) corresponds to the model outputs associated with a specific hydrological process of the nth grid. Within $\mathbf{W}_n$, each row represents a rainy day under consideration, with i denoting the total number of rainy days analyzed. Each row comprises three values: the daily model output y_{kn} (k=1, 2, …, i), the corresponding rainfall amount p_k (k=1, 2, …, i), and the grid's slope angle s_n. Consequently, the Spearman correlation coefficient was computed between the transpose vectors $\boldsymbol{y}_{N\times i}^{\boldsymbol{T}}$ and $\boldsymbol{s}_{N\times i}^{\boldsymbol{T}}$.

To analyze LULCC effects, vectors $\boldsymbol{H}_{\mathrm{d}}$ (Eq. (B3)) and $\boldsymbol{C}_{\mathrm{d}}$ (Eq.(B4)) were generated for each grid under HLU and CLU patterns, and the KS test value was computed between these two vectors for each grid,

$$\boldsymbol{H}_{\boldsymbol{d}} = \left[y_{1|\mathrm{HLU}}, y_{2|\mathrm{HLU}}, \cdots, y_{i|\mathrm{HLU}}\right], \tag{B3}$$

$$\boldsymbol{C}_{\boldsymbol{d}} = \left[y_{1|\mathrm{CLU}}, y_{2|\mathrm{CLU}}, \cdots, y_{i|\mathrm{CLU}}\right], \tag{B4}$$

where i denotes the total number of rainy days, $y_{k|\mathrm{HLU}}$ and $y_{k|\mathrm{CLU}}$ (k=1, 2, …, i) represent the model daily output of this grid under the HLU pattern and the CLU pattern on the kth rainy day, respectively. We also calculated the absolute difference in mean values of these two vectors to quantify the magnitude of change between the two land use patterns in terms of their effects on the model outputs.

To evaluate the effects of slope on an annual scale, a new matrix **A** is constructed as following Eq. (B5):

$$\mathbf{A} = \begin{bmatrix} y_1 & s_1 \\ \vdots & \vdots \\ y_N & s_N \end{bmatrix}, \tag{B5}$$

where N represents the number of grids within each zone, y_n and s_n (n=1, 2, …, N) denote the annual output and slope angle for the nth grid, respectively. Only grids with annual volumes exceeding 10 mm were considered for surface runoff and subsurface flow analysis to concentrate on pronounced flows. Subsequently, the Spearman correlation coefficient was calculated between the transpose vectors $\boldsymbol{y}_N^{\mathrm{T}}$ and $\boldsymbol{s}_N^{\mathrm{T}}$.

https://doi.org/10.5194/hess-2024-136
Preprint. Discussion started: 17 June 2024

Hydrology and Earth System Sciences
Discussions
Open Access
EGU

The KS test was also applied at the annual scale to compare model outputs between HLU and CLU patterns across the entire subbasin range. Vectors $\boldsymbol{H}_{\mathrm{y}}$ (Eq. (B6)) and $\boldsymbol{C}_{\mathrm{y}}$ (Eq. (B7)) represent the annual model outputs under the HLU pattern and the CLU pattern, respectively.

$$\boldsymbol{H}_{\mathrm{y}} = \left[y_{1|\mathrm{HLU}}, y_{2|\mathrm{HLU}}, \cdots, y_{j|\mathrm{HLU}}\right], \tag{B6}$$

$$\boldsymbol{C}_{\mathrm{y}} = \left[y_{1|\mathrm{CLU}}, y_{2|\mathrm{CLU}}, \cdots, y_{j|\mathrm{CLU}}\right], \tag{B7}$$

Here z denotes the number of grids across each subbasin, $y_{k|\mathrm{HLU}}$ and $y_{k|\mathrm{CLU}}$ (k=1, 2, …, z) represent the model annual output of the kth grid under the HLU pattern and the CLU pattern, respectively. Then the KS test was carried out between these two vectors.

Appendix C: Supplementary calibration results

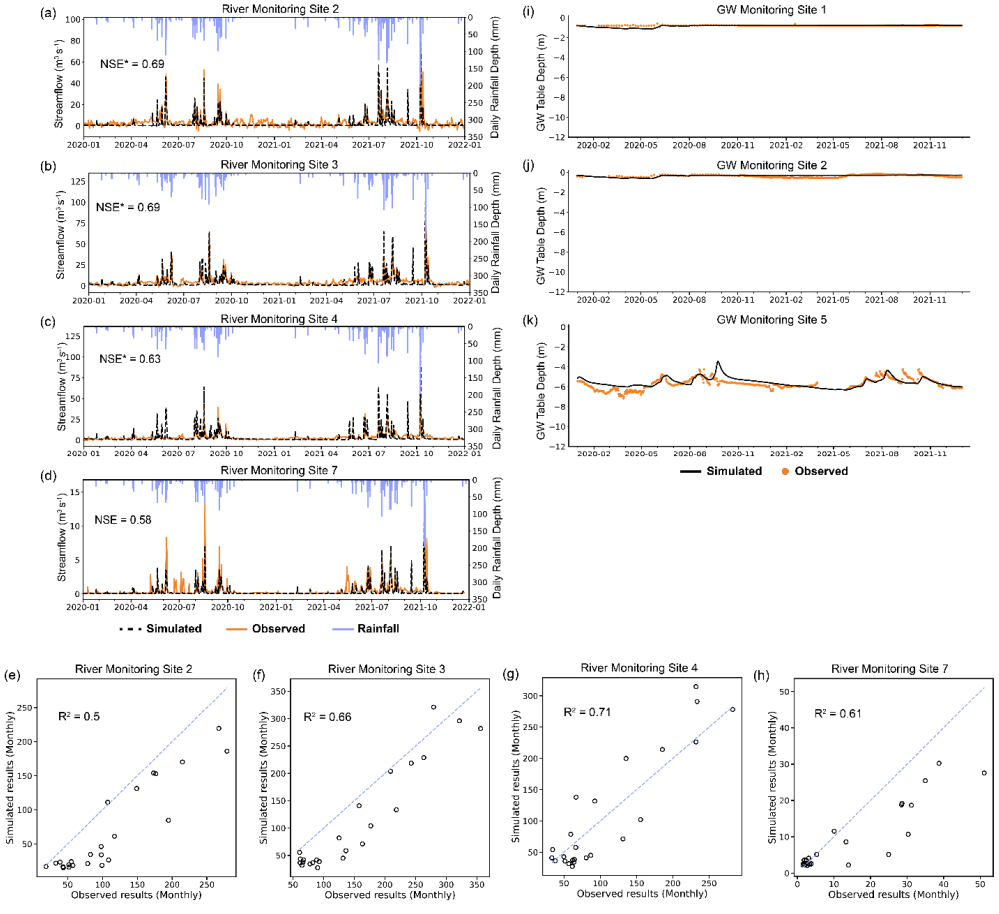

Figure C1. Other sites calibration results across daily river discharge (a)–(d), and monthly river discharge (e)–(h), and groundwater table depth (i)–(k).

https://doi.org/10.5194/hess-2024-136
Preprint. Discussion started: 17 June 2024

Hydrology and Earth System Sciences
Discussions

454 **Table C1.** Spearman coefficients between infiltration and subsurface flow.

	Zone 1	Zone 2	Zone 3
Daily scale			
NTRW	-	-	0.20
BJRW	0.19	-	-
Annual scale			
NTRW	0.67	0.68	0.72
BJRW	0.82	0.66	0.77

455

456 *Code and data availability.* The source code of the SHUD model can be downloaded from https://github.com/SHUD-
457 System/SHUD. The model spatial input data are freely available from the described source listed in Table 1. The
458 meteorological data and monitoring data in this study can be obtained upon request.

459

460 *Author contributions.* HL contributed to methodology, validation, visualization, writing of the original draft and editing. HY
461 contributed to data collection, reviewing and editing the original draft. MG contributed to conceptualization, supervision,
462 methodology, writing, reviewing and editing the original draft.

463

464 *Competing interests.* The authors declare that they have no conflicts of interest.

465

466 *Acknowledgements.* This work is financially supported by General Research Fund projects (No. 17210923).

467 **References**

468 Ayalew, T. B., Krajewski, W. F., and Mantilla, R.: Insights into expected changes in regulated flood frequencies due to the
469 spatial configuration of flood retention ponds, J. Hydrol. Eng., 20(10), 04015010, https://doi.org/10.1061/(ASCE)HE.1943-
470 5584.0001229, 2015.
471 Baroni, G., Facchi, A., Gandolfi, C., Ortuani, B., Horeschi, D., and van Dam, J. C.: Uncertainty in the determination of soil
472 hydraulic parameters and its influence on the performance of two hydrological models of different complexity, Hydrol.
473 Earth Syst. Sci., 14, 251–270, https://doi.org/10.5194/hess-14-251-2010, 2010.
474 Bai, P., Liu, X., Zhang, Y., and Liu, C.: Assessing the impacts of vegetation greenness change on evapotranspiration and water
475 yield in China, Water Resour. Res., 56(10), e2019WR027019, https://doi.org/10.1029/2019WR027019, 2020.
476 Bear, J.: Dynamics of fluids in porous media. Dover Publications, 2013.
477 Beven, K.J., Rainfall-runoff modelling: the primer, John Wiley & Sons, 2011.
478 Beven, K. J., and Kirkby, M. J.: A physically based, variable contributing area model of basin hydrology, Hydrological Sciences
479 Bulletin, 24(1), 43–69, https://doi.org/10.1080/02626667909491834, 1979.
480 Beven, K. J, Young, P., Romanowicz, R., O'Connell, P. E., Ewen, J., O'Donnell, G., Holman, I., Posthumus, H., Morris, J.,
481 Hollis, J., Rose, S., Lamb, R., and Archer, D.: Analysis of historical data sets to look for impacts of land use and management

https://doi.org/10.5194/hess-2024-136
Preprint. Discussion started: 17 June 2024

change on flood generation, Final Report FD2120, Defra, London, 2008.

Bosch, J. M. and Hewlett, J. D.: A review of catchment experiments to determine the effect of vegetation changes on water yield and evapotranspiration, J. Hydrol., 55, 3-23, https://doi.org/10.1016/0022-1694(82)90117-2, 1982.

Brath, A., Montanari, A., and Moretti, G.: Assessing the effect on flood frequency of land use change via hydrological simulation (with uncertainty), J. Hydrol., 324, 141-153, https://doi.org/10.1016/j.jhydrol.2005.10.001, 2006.

Brandhorst, N. and Neuweiler, I.: Impact of parameter updates on soil moisture assimilation in a 3D heterogeneous hillslope model, Hydrol. Earth Syst. Sci., 27, 1301–1323, https://doi.org/10.5194/hess-27-1301-2023, 2023.

Brown, A. E., Zhang, L., McMahon, T. A., Western, A. W., and Vertessy, R. A.: A review of paired catchment studies for determining changes in water yield resulting from alterations in vegetation, J. Hydrol., 310, 28-61, https://doi.org/10.1016/j.jhydrol.2004.12.010, 2005.

Brown, C. F., Brumby, S. P., Guzder-Williams, B., and et al.: Dynamic World, Near real-time global 10 m land use land cover mapping, Sci. Data, 9, 251, https://doi.org/10.1038/s41597-022-01307-4, 2022.

Camporese, M., Paniconi, C., Putti, M., and McDonnell, J. J.: Fill and Spill Hillslope Runoff Representation With a Richards Equation-Based Model, Water Resour. Res., 55, 8445-8462, https://doi.org/10.1029/2019WR025726, 2019.

Cheng, J., Chen, M., and Tang, S.: Shenzhen – A typical benchmark of Chinese rapid urbanization miracle, Cities, 140, 104421, https://doi.org/10.1016/j.cities.2023.104421, 2023.

Chu, H.-J., Lin, Y.-P., Huang, C.-W., Hsu, C.-Y., and Chen, H.-Y.: Modelling the hydrologic effects of dynamic land-use change using a distributed hydrologic model and a spatial land-use allocation model, Hydrol. Process., 24, 2538-2554, https://doi.org/10.1002/hyp.7667, 2010.

Costa, M. H., Botta, A., and Cardille, J. A.: Effects of large-scale changes in land cover on the discharge of the Tocantins River, Southeastern Amazonia, J. Hydrol., 283, 206-217, https://doi.org/10.1016/S0022-1694(03)00267-1, 2003.

Das, B. M.: Principles of geotechnical engineering, Brooks Cole/Thompson Learning, 1990.

Detty, J. M. and McGuire, K. J.: Topographic controls on shallow groundwater dynamics: implications of hydrologic connectivity between hillslopes and riparian zones in a till mantled catchment, Hydrol. Process., 24, 2222-2236, https://doi.org/10.1002/hyp.7656, 2010.

Diem, J. E., Pangle, L. A., Milligan, R. A., and Adams, E. A.: Intra-annual variability of urban effects on streamflow, Hydrol. Process., 35(9), e14371, https://doi.org/10.1002/hyp.14371, 2021.

Du, J., Qian, L., Rui, H., Zuo, T., Zheng, D., Xu, Y., and Xu, C. Y.: Assessing the effects of urbanization on annual runoff and flood events using an integrated hydrological modeling system for Qinhuai River basin, China, J. Hydrol., 464, 127-139, https://doi.org/10.1016/j.jhydrol.2012.07.007, 2012.

Fan, Y., Clark, M., Lawrence, D. M., Swenson, S., Band, L. E., Brantley, S. L., et al.: Hillslope hydrology in global change research and Earth system modeling, Water Resour. Res., 55, 1737-1772, https://doi.org/10.1029/2018WR023903, 2019.

Fatichi, S., Vivoni, E. R., Ogden, F. L., Ivanov, V. Y., Mirus, B., Gochis, D., ... and Tarboton, D.: An overview of current applications, challenges, and future trends in distributed process-based models in hydrology, J. Hydrol., 537, 45-60, https://doi.org/10.1016/j.jhydrol.2016.03.026, 2016.

Freeze, R.A. and Cherry, J.A.: Groundwater, Prentice Hall, Inc.,Englewood Cliffs, N.J., 1979.

Garg, V., Aggarwal, S. P., Gupta, P. K., Nikam, B. R., Thakur, P. K., Srivastav, S. K., and Senthil Kumar, A.: Assessment of land use land cover change impact on hydrological regime of a basin, Environ. Earth Sci., 76, 1-17, https://doi.org/10.1007/s12665-016-6389-3, 2017.

Gao, H., Birkel, C., Hrachowitz, M., Tetzlaff, D., Soulsby, C., and Savenije, H. H. G.: A simple topography-driven and calibration-free runoff generation module, Hydrol. Earth Syst. Sci., 23, 787–809, https://doi.org/10.5194/hess-23-787-2019, 2019.

GeoCloud: https://geocloud.cgs.gov.cn/, last access: 02 April 2024.

Guan, M., Sillanpää, N., and Koivusalo, H.: Modelling and assessment of hydrological changes in a developing urban catchment, Hydrol. Process., 29, 2880-2894, https://doi.org/10.1002/hyp.10410, 2015.

https://doi.org/10.5194/hess-2024-136
Preprint. Discussion started: 17 June 2024

527 Guo, K., Guan, M., Yan, H., and Xia, X.: A spatially distributed hydrodynamic model framework for urban flood hydrological
528 and hydraulic processes involving drainage flow quantification, J. Hydrol., 625, 130-135,
529 https://doi.org/10.1016/j.jhydrol.2023.130135, 2023.
530 Gwak, Y. and Kim, S.: Factors affecting soil moisture spatial variability for a humid forest hillslope, Hydrol. Process., 31, 431–
531 445, https://doi.org/10.1002/hyp.11064, 2017.
532 Hauke, J. and Kossowski, T.: Comparison of Values of Pearson's and Spearman's Correlation Coefficients on the Same Sets of
533 Data, Quaest. Geogr., 30(2), 87-93, https://doi.org/10.2478/v10117-011-0021-1, 2011.
534 Hopp, L. and McDonnell, J. J.: Connectivity at the hillslope scale: Identifying interactions between storm size, bedrock
535 permeability, slope angle and soil depth, J. Hydrol., 376, 378-391, https://doi.org/10.1016/j.jhydrol.2009.07.047, 2009.
536 Im, S., Kim, H., Kim, C., and Jang, C.: Assessing the impacts of land use changes on watershed hydrology using MIKE SHE,
537 Environ. Geol., 57, 231-239, https://doi.org/10.1007/s00254-008-1303-3, 2009.
538 Jarecke, K. M., Bladon, K. D., and Wondzell, S. M.: The influence of local and nonlocal factors on soil water content in a steep
539 forested catchment, Water Resour. Res., 57(5), e2020WR028343, https://doi.org/10.1029/2020WR028343, 2021.
540 Jencso, K. G., and McGlynn, B. L.: Hierarchical controls on runoff generation: Topographically driven hydrologic connectivity,
541 geology, and vegetation, Water Resour. Res., 47, W11527, https://doi.org/10.1029/2011WR010666, 2011.
542 Kumar, M.: Toward a Hydrologic Modeling System, Ph.D. Thesis, The Pennsylvania State University, 273 pp., 2009.
543 Kumar, M., Duffy, C. J., and Salvage, K. M.: A Second-Order Accurate, Finite Volume–Based, Integrated Hydrologic Modeling
544 (FIHM) Framework for Simulation of Surface and Subsurface Flow, Vadose Zone J., 8, 873-890,
545 https://doi.org/10.2136/vzj2009.0014, 2009.
546 Kumar, M., Denis, D. M., Kundu, A., Joshi, N., and Suryavanshi, S.: Understanding land use/land cover and climate change
547 impacts on hydrological components of Usri watershed, India, Appl. Water Sci., 12(3), 39, https://doi.org/10.1007/s13201-
548 022-01662-3, 2022.
549 Larson, J., Lidberg, W., Ågren, A. M., and Laudon, H.: Predicting soil moisture conditions across a heterogeneous boreal
550 catchment using terrain indices, Hydrol. Earth Syst. Sci., 26, 4837-4851, https://doi.org/10.5194/hess-26-4837-2022, 2022.
551 Li, Z., Liu, W.-z., Zhang, X.-c., and Zheng, F.-l.: Impacts of land use change and climate variability on hydrology in an
552 agricultural catchment on the Loess Plateau of China, J. Hydrol., 377, 35-42, https://doi.org/10.1016/j.jhydrol.2009.08.007,
553 2009.
554 Liang, C., and Guan, M.: Effects of urban drainage inlet layout on surface flood dynamics and discharge, J. Hydrol., 130890,
555 https://doi.org/10.1016/j.jhydrol.2024.130890, 2024.
556 Lilliefors, H. W.: On the Kolmogorov-Smirnov test for normality with mean and variance unknown, J. Am. Stat. Assoc.,
557 62(318), 399-402, https://doi.org/10.2307/2283970, 1967.
558 Liu, J., Zhang, Q., Singh, V. P., and Shi, P.: Contribution of multiple climatic variables and human activities to streamflow
559 changes across China, J. Hydrol., 545, 145-162, https://doi.org/10.1016/j.jhydrol.2016.12.048, 2017.
560 Liu, H., Dai, H., Niu, J., Hu, B. X., Gui, D., Qiu, H., Ye, M., Chen, X., Wu, C., Zhang, J., and Riley, W.: Hierarchical sensitivity
561 analysis for a large-scale process-based hydrological model applied to an Amazonian watershed, Hydrol. Earth Syst. Sci.,
562 24, 4971–4996, https://doi.org/10.5194/hess-24-4971-2020, 2020.
563 Maxwell, R. M., Putti, M., Meyerhoff, S., Delfs, J.-O., Ferguson, I. M., Ivanov, V., Kim, J., Kolditz, O., Kollet, S. J., Kumar,
564 M., Lopez, S., Niu, J., Paniconi, C., Park, Y.-J., Phanikumar, M. S., Shen, C., Sudicky, E. A., and Sulis, M.: Surface-
565 subsurface model intercomparison: a first set of benchmark results to diagnose integrated hydrology and feedbacks, Water
566 Resour. Res., 50, 1531–1549, https://doi.org/10.1002/2013wr013725, 2014.
567 Mirus, B. B. and Loague, K.: How runoff begins (and ends): Characterizing hydrologic response at the catchment scale, Water
568 Resour. Res., 49, 2987-3006, https://doi.org/10.1002/wrcr.20218, 2013.
569 Moriasi, D. N., Arnold, J. G., Van Liew, M. W., Bingner, R. L., Harmel, R. D., and Veith, T. L.: Model evaluation guidelines
570 for systematic quantification of accuracy in watershed simulations, Trans. ASABE, 50(3), 885-900, 2007.
571 Neal, J. and Hawker, L. (Creators), Uhe, P., Paulo, L., Sosa, J., Savage, J., Sampson, C. (Contributors). FABDEM V1-2.

https://doi.org/10.5194/hess-2024-136
Preprint. Discussion started: 17 June 2024

University of Bristol. https://doi.org/10.5523/bris.s5hqmjcdj8yo2ibzi9b4ew3sn, 2023.

Niehoff, D., Fritsch, U., and Bronstert, A.: Land-use impacts on storm-runoff generation: scenarios of land-use change and simulation of hydrological response in a meso-scale catchment in SW-Germany, J. Hydrol., 267, 80-93, https://doi.org/10.1016/S0022-1694(02)00142-7, 2002.

Niu, J., Shen, C., Chambers, J. Q., Melack, J. M., and Riley, W. J.: Interannual variation in hydrologic budgets in an Amazonian watershed with a coupled subsurface–land surface process model, J. Hydrometeorol., 18(9), 2597-2617, https://doi.org/10.1175/JHM-D-16-0253.1, 2017.

Nobre, A. D., Cuartas, L. A., Hodnett, M., Rennó, C. D., Rodrigues, G., Silveira, A., and Saleska, S.: Height Above the Nearest Drainage–a hydrologically relevant new terrain model, J. Hydrol., 404(1-2), 13-29, https://doi.org/10.1016/j.jhydrol.2011.03.051, 2011.

O'Loughlin, E. M.: Prediction of Surface Saturation Zones in Natural Catchments by Topographic Analysis, Water Resour. Res., 22(5), 794–804, https://doi.org/10.1029/WR022i005p00794, 1986.

Olang, L. O. and Fürst, J.: Effects of land cover change on flood peak discharges and runoff volumes: model estimates for the Nyando River Basin, Kenya, Hydrol. Process., 25, 80-89, https://doi.org/10.1002/hyp.7821, 2011.

Pang, X., Gu, Y., Launiainen, S., and Guan, M.: Urban hydrological responses to climate change and urbanization in cold climates, Science of the Total Environment, 817, 153066, 2022.

Qu, Y. and Duffy, C. J.: A semidiscrete finite volume formulation for multiprocess watershed simulation, Water Resour. Res., 43, W08419, https://doi.org/10.1029/2006WR005752, 2007.

RESDC: https://www.resdc.cn/Default.aspx, last access: 02 April 2024.

Rinderer, M., van Meerveld, H. J., and Seibert, J.: Topographic controls on shallow groundwater levels in a steep, prealpine catchment: When are the TWI assumptions valid?, Water Resour. Res., 50, 6067–6080, https://doi.org/10.1002/2013WR015009, 2014.

Seibert, J., Bishop, K., Rodhe, A., and McDonnell, J. J.: Groundwater dynamics along a hillslope: A test of the steady state hypothesis, Water Resour. Res., 39, 1, https://doi.org/10.1029/2002WR001404, 2003.

Shao, M., Zhao, G., Kao, S. C., Cuo, L., Rankin, C., and Gao, H.: Quantifying the effects of urbanization on floods in a changing environment to promote water security—A case study of two adjacent basins in Texas, J. Hydrol., 589, 125154, https://doi.org/10.1016/j.jhydrol.2020.125154, 2020.

Shen, C., and Phanikumar, M. S.: A process-based, distributed hydrologic model based on a large-scale method for surface–subsurface coupling, Adv. Water Resour., 33(12), 1524-1541, https://doi.org/10.1016/j.advwatres.2010.09.002, 2010.

Shi, Y., Davis, K. J., Zhang, F., Duffy, C. J., and Yu, X.: Parameter estimation of a physically based land surface hydrologic model using the ensemble Kalman filter: A synthetic experiment, Water Resour. Res., 50, 706-724, https://doi.org/10.1002/2013WR014070, 2014.

Shu, L., Ullrich, P. A., and Duffy, C. J.: Simulator for Hydrologic Unstructured Domains (SHUD v1.0): numerical modeling of watershed hydrology with the finite volume method, Geosci. Model Dev., 13, 2743–2762, https://doi.org/10.5194/gmd-13-2743-2020, 2020.

Shu, L., Ullrich, P., Meng, X., Duffy, C., Chen, H., and Li, Z.: rSHUD v2.0: advancing the Simulator for Hydrologic Unstructured Domains and unstructured hydrological modeling in the R environment, Geosci. Model Dev., 17, 497–527, https://doi.org/10.5194/gmd-17-497-2024, 2024.

SHUD Book: https://www.shud.xyz/book_en/, last access: 02 April 2024.

Sicaud, E., Fortier, D., Dedieu, J.-P., and Franssen, J.: Pairing remote sensing and clustering in landscape hydrology for large-scale change identification: an application to the subarctic watershed of the George River (Nunavik, Canada), Hydrol. Earth Syst. Sci., 28, 65–86, https://doi.org/10.5194/hess-28-65-2024, 2024.

Singh, N. K., Emanuel, R. E., McGlynn, B. L., and Miniat, C. F.: Soil moisture responses to rainfall: Implications for runoff generation, Water Resour. Res., 57, e2020WR028827, https://doi.org/10.1029/2020WR028827, 2021.

Smith, J. A., Cox, A. A., Baeck, M. L., Yang, L., and Bates, P.: Strange floods: The upper tail of flood peaks in the United

https://doi.org/10.5194/hess-2024-136
Preprint. Discussion started: 17 June 2024

Hydrology and Earth System Sciences
Discussions

States, Water Resour. Res., 54(9), 6510-6542, https://doi.org/10.1002/2018WR023536, 2018.

Song, X., Zhang, J., Zhan, C., Xuan, Y., Ye, M., and Xu, C.: Global sensitivity analysis in hydrological modeling: Review of concepts, methods, theoretical framework, and applications, J. Hydrol., 523, 739-757, https://doi.org/10.1016/j.jhydrol.2015.02.013, 2015.

Sørensen, R., Zinko, U., and Seibert, J.: On the calculation of the topographic wetness index: evaluation of different methods based on field observations, Hydrol. Earth Syst. Sci., 10, 101–112, https://doi.org/10.5194/hess-10-101-2006, 2006.

Strahler, A. N.: Quantitative analysis of watershed geomorphology, Eos Trans. AGU, 38, 913-920, https://doi.org/10.1029/TR038i006p00913, 1957.

Thanapakpawin, P., Richey, J., Thomas, D., Rodda, S., Campbell, B., and Logsdon, M.: Effects of landuse change on the hydrologic regime of the Mae Chaem river basin, NW Thailand, J. Hydrol., 334, 215-230, https://doi.org/10.1016/j.jhydrol.2006.10.012, 2007.

Thornton, J. M., Therrien, R., Mariéthoz, G., Linde, N., and Brunner, P.: Simulating fully-integrated hydrological dynamics in complex Alpine headwaters: Potential and challenges, Water Resour. Res., 58, e2020WR029390, https://doi.org/10.1029/2020WR029390, 2022.

Van Genuchten, M.T.: A Closed-form equation for predicting the hydraulic conductivity of unsaturated soils. Soil Science Society of America Journal, 44: 892-898. https://doi.org/10.2136/sssaj1980.03615995004400050002x, 1980.

Van Loon, A. F., Rangecroft, S., Coxon, G., Breña Naranjo, J. A., Van Ogtrop, F., and Van Lanen, H. A. J.: Using paired catchments to quantify the human influence on hydrological droughts, Hydrol. Earth Syst. Sci., 23, 1725–1739, https://doi.org/10.5194/hess-23-1725-2019, 2019.

Yan, H., Guan, M., and Kong, Y.: Flood Retention Lakes in a Rural-Urban Catchment: Climate-Dominated and Configuration-Affected Performances, Water Resour. Res., 59(8), e2022WR032911, https://doi.org/10.1029/2022WR032911, 2023.

Yan, H., Gao, Y., Wilby, R., Yu, D., Wright, N., Yin, J., ... and Guan, M.: Urbanization further intensifies short-duration rainfall extremes in a warmer climate, Geophys. Res. Lett., 51(5), e2024GL108565, https://doi.org/10.1029/2024GL108565, 2024.

Yang, L., Smith, J. A., Baeck, M. L., and Zhang, Y.: Flash flooding in small urban watersheds: Storm event hydrologic response, Water Resour. Res., 52(6), 4571-4589, https://doi.org/10.1002/2016WR018699, 2016.

Yang, L., Smith, J., and Niyogi, D.: Urban impacts on extreme monsoon rainfall and flooding in complex terrain, Geophys. Res. Lett., 46(11), 5918-5927, https://doi.org/10.1029/2019GL083315, 2019.

Yin, J., Gao, Y., Chen, R., Yu, D., Wilby, R., Wright, N., ... and Guan, M.: Flash floods: why are more of them devastating the world's driest regions?, J. Hydrol., 15, 225-240, https://doi.org/10.1234/jh.2023.15123, 2023.

Yu, X., Luo, L., Hu, P., Tu, X., Chen, X., and Wei, J.: Impacts of sea-level rise on groundwater inundation and river floods under changing climate, J. Hydrol., 614, 128554, https://doi.org/10.1016/j.jhydrol.2022.128554, 2022.

Zanetti, F., Botter, G., and Camporese, M.: Stream Network Dynamics of Non-Perennial Rivers: Insights From Integrated Surface-Subsurface Hydrological Modeling of Two Virtual Catchments, Water Resour. Res., 60, e2023WR035631, https://doi.org/10.1029/2023WR035631, 2024.

Zhang, M., Liu, N., Harper, R., Li, Q., Liu, K., Wei, X., ... and Liu, S.: A global review on hydrological responses to forest change across multiple spatial scales: Importance of scale, climate, forest type and hydrological regime, J. Hydrol., 546, 44-59, https://doi.org/10.1016/j.jhydrol.2017.01.024, 2017.

Zhang, X., Jiao, J. J., and Guo, W.: How Does Topography Control Topography-Driven Groundwater Flow?, Geophys. Res. Lett., 49, e2022GL101005, https://doi.org/10.1029/2022GL101005, 2022a.

Zhang, J., Zhang, Y., Sun, G., Song, C., Li, J., Hao, L., and Liu, N.: Climate variability masked greening effects on water yield in the Yangtze River Basin during 2001–2018, Water Resour. Res., 58(1), e2021WR030382, https://doi.org/10.1029/2021WR030382, 2022b.

Zhou, G., Wei, X., Chen, X., Zhou, P., Liu, X., Xiao, Y., Sun, G., Scott, D. F., Zhou, S., Han, L., and Su, Y.: Global pattern for the effect of climate and land cover on water yield, Nat. Commun., 6, 5918, https://doi.org/10.1038/ncomms6918, 2015.